Journal of ELECTRONIC MATERIALS, Vol. 50, No. 3, 2021
https://doi.org/10.1007/s11664-020-08498-9

Time-Lapse Imaging of Ag_3Sn Thermal Coarsening in Sn-3Ag-0.5Cu Solder Joints

J.W. XIAN ,[1,2] S.A. BELYAKOV,[1] and C.M. GOURLAY[1]

1.—Department of Materials, Imperial College, London SW7 2AZ, UK. 2.—e-mail: j.xian@imperial.ac.uk

The coarsening of Ag_3Sn particles occurs during the operation of joints and plays an important role in failure. Here, Ag_3Sn coarsening is studied at 125°C in the eutectic regions of Sn-3Ag-0.5Cu/Cu solder joints by SEM-based time-lapse imaging. Using multi-step thresholding segmentation and image analysis, it is shown that coalescence of Ag_3Sn particles is an important ripening process in addition to LSW-like Ostwald ripening. About 10% of the initial Ag_3Sn particles coalesced during ageing, coalescence occurred uniformly across eutectic regions, and the scaled size distribution histograms contained large particles that can be best fit by the Takajo model of coalescence ripening. Similar macroscopic coarsening kinetics were measured between the surface and bulk Ag_3Sn particles. Tracking of individual surface particles showed an interplay between the growth/shrinkage and coalescence of Ag_3Sn.

Key words: Soldering, intermetallics, precipitates, coarsening, time-lapse imaging

INTRODUCTION

Ag_3Sn particles are a primary strengthening mechanism in Sn-Ag and Sn-Ag-Cu (SAC) solder joints,[1,2] and their coarsening in-service plays an important role in solder joint failure.[3] During thermal cycling, Ag_3Sn particle coarsening has two components: thermal coarsening, and strain-enhanced coarsening. Various studies have shown that accelerated coarsening of Ag_3Sn particles occurs in regions of stress concentration which is often in the solder near the package side, and results in a local loss of strength and is a precursor to crack initiation in this region.[4–9] Ag_3Sn coarsening is relatively rapid in solder joints because they are cycled through a homologous temperature range of up to $T/Tm \sim 0.5$–0.8, and thermal coarsening of Ag_3Sn is a significant challenge in applications where high reliability is required at high maximum operation temperature (e.g. at 125°C).

(Received July 14, 2020; accepted September 17, 2020; published online October 13, 2020)

The Ag_3Sn particles that give strengthening initially form in a eutectic reaction during solidification and then their size and shape continue to develop in service due to the relatively high homologous temperature. The sizes of Ag_3Sn particles after soldering are typically submicron in a range of Sn-Ag-Cu solders,[10–18] which can greatly improve the strength and creep resistance of solders through precipitate strengthening. A wide range of eutectic Ag_3Sn sizes (from ~ 80 nm to ~ 500 nm) are reported for solders containing similar concentration of Ag[12–18] which is related to differences in cooling rate,[12–16] nucleation undercooling for β-Sn,[19] and imaging quality of electron microscopy.[16,17] These factors are a challenge for studying Ag_3Sn coarsening and highlight the need to apply well-controlled solidification conditions including the nucleation undercooling for β-Sn in sample preparation, and suitable imaging and quantification approaches to measure the ~ 100 nm particles.

Coarsening of eutectic Ag_3Sn generally causes significant and problematic microstructural changes, including increasing size of eutectic Ag_3Sn particles in the bulk[18,20,21] and near the

intermetallic layers.[22–24] The study of the Ag_3Sn coarsening process can provide insights to better understand the failure of solder joints, and a good quantitative understanding of Ag_3Sn particle coarsening is required to build future microstructure-level models of thermal cycling. There have been time-lapse studies[11,25] directly observing Ag_3Sn coarsening in fixed regions, with an initial size of $\sim$ 350 nm in as-solidified Sn-3.5Ag-0.5Cu (SAC305). Fu et al.[11] reported the growth, disappearance, coalescence and splitting of Ag_3Sn particles by comparing aligned micrographs. However, a more quantitative analysis of microstructural evolution is needed, and comparisons between the coarsening kinetics on a polished surface versus in the bulk solder are required to validate the approach.

In this work, we investigate the mechanisms of thermal coarsening of Ag_3Sn particles in SAC305 at 125°C using time-lapse imaging. An automated segmentation method is developed for faster and more accurate quantification of the particle sizes. The coarsening kinetics and size distributions obtained on the surface are then compared with those obtained in the bulk solders to test the validity of the results. Quantification of changes in individual particles in time-lapse images is then carried out to investigate the interplay between coarsening and coalescence of Ag_3Sn particles.

METHODS

Sn-3Ag-0.5Cu (in mass%) alloy was made by melting 99.9Sn, 99.9Ag and a Sn-10Cu master alloy in a high-purity graphite crucible and casting. The ingots were then rolled down to foils and punched into disks weighing about 0.5 mg each. The disks were remelted in ROL-1 tacky flux on an inert sheet using a hot plate at 350°C, to form liquid spheres due to surface tension, generating $\sim$ 500 μm BGA solder balls once solidified. BGA balls were soldered onto Cu-OSP pads on PCBs by reflowing in a LFR400HTX TORNARDO reflow oven (Surface Mount Technology, Isle of Wight, UK) with a peak temperature of $\sim$ 245°C.[26] To ensure a precise thermal profile and measure the nucleation undercooling for β-Sn, the samples were then reflowed again in a Mettler Toledo differential scanning calorimeter by heating at 0.16 K/s to 240°C followed by cooling at 0.33 K/s. Only joints that solidified with an undercooling in the range 20 $\pm$ 2 K were kept for subsequent coarsening studies to ensure similar solidification conditions in each joint, to have a similar initial eutectic Ag_3Sn size in each joint.

The remaining as-solidified joints were then divided into two groups and prepared differently for coarsening kinetics studies in the bulk and on the surface. The group for the bulk coarsening study were aged at 125°C from 0 h (as-solidified) up to 6 months, then mounted in Struers VersoCit acrylic cold mounting resin. After standard metallographic procedures, a Zeiss Auriga field emission gun scanning electron microscope (FEG-SEM) was used for imaging. The other group for surface coarsening investigation was glued on cylindrical specimen stubs and then inserted in a Gatan Disc Grinder for manual metallographic preparation. This resin-free method was used to eliminate the problems of resin deformation and degradation during ageing at 125°C (i.e. causing deformation or contamination on the solder surface). The as-solidified sample was initially imaged in the SEM and then re-imaged repeatedly after different ageing times in a 125°C furnace outside the SEM chamber. The images taken from different SEM sessions were then aligned using Linear Stack Alignment with the Scale Invariant Feature Transform (SIFT) in Image J software.[27]

The image segmentation method used is summarised in Fig. 1. A low-magnification image is shown in Fig. 1a. The black particles are Cu_6Sn_5 and the lighter particles are Ag_3Sn. A simple thresholding method cannot segment the Ag_3Sn particles properly as can be seen in the red mask in Fig. 1b. An improved blue mask using a multi-step thresholding is shown in Fig. 1c, and the white arrows point out a few larger Ag_3Sn particles that were missed in Fig. 1b. The multi-step thresholding method is overviewed in Fig. 1d, e, f, g, h, and i at a higher magnification. Figure 1e shows an initial edge detection result outlining the Ag_3Sn particles with clear boundaries against the background. In Fig. 1f the particles with closed edges are filled and the partially open ones left unfilled. In Fig. 1g, the partially open edges are then expanded at endpoints using squares of pixels, followed by skeletonization to bridge the narrow openings. The newly closed particles are then filled in Fig. 1h. A final step to capture some small particles was used and included in the mask shown in Fig. 1i, noting that particles on image borders are excluded. This segmentation method was automated in Matlab, allowing a large number of images to be sampled. This multi-step thresholding has improved the accuracy and reproducibility of the quantification of Ag_3Sn particle size.

RESULTS AND DISCUSSION

Microstructural Evolution and Size Distributions of Ag_3Sn Particles During Ageing

Figure 2 shows cross-sectional BSE micrographs at increasing magnifications in as-solidified SAC305/Cu solder joints. There are a few large hexagonal primary Cu_6Sn_5 crystals in the BGA ball in Fig. 2a and no primary Ag_3Sn crystals are found in the sample. This is because Cu is dissolved from the substrate and the consistent nucleation undercooling for β-Sn (20 $\pm$ 2 K) gives a reproducible solidification sequence of primary Cu_6Sn_5, followed by β-Sn dendrites and then eutectic reactions

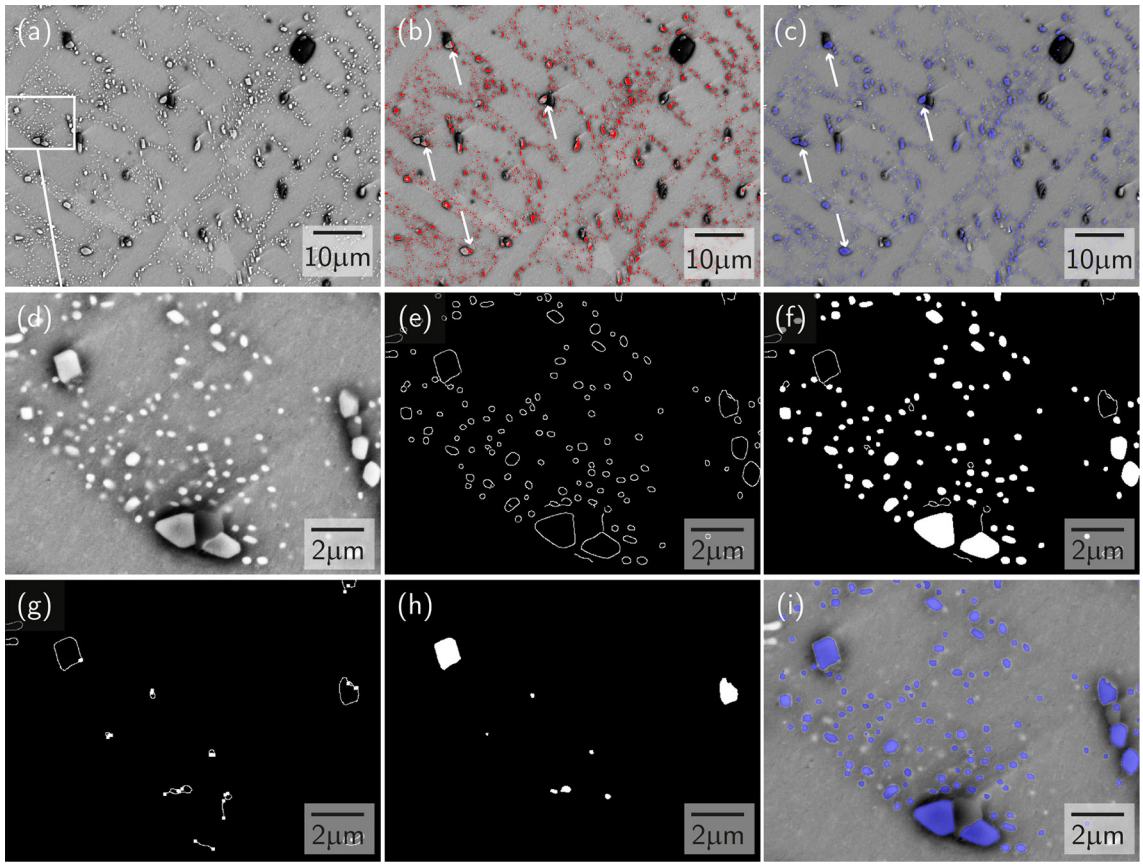

Fig. 1. Image segmentation. (a) Low-magnification image of as-solidified SAC305/Cu, superimposed with (b) red segmentation using simple thresholding and (c) blue segmentation using multi-step thresholding. The multiple steps used include (d) raw image, (e) finding edges, (f) filling closed edges, (g) expanding endpoints of opening edges, (h) filling newly closed edges, (i) filled particles superimposed on the raw image (Color figure online).

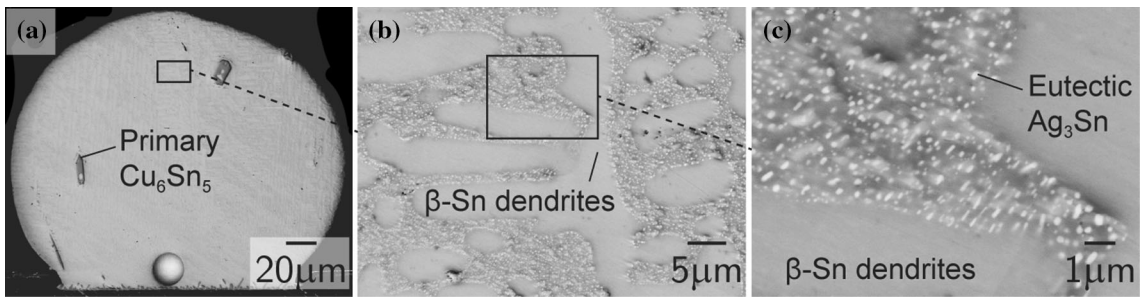

Fig. 2. Microstructures of as-solidified SAC305/Cu solder joints at increasing magnification, showing (a) a whole BGA joint, (b) β-Sn dendrites and (c) eutectic Ag_3Sn particles.

involving β-Sn, Cu_6Sn_5 and Ag_3Sn. The volume fraction of Ag_3Sn is predicted to be about 3.0% using Thermo-Calc 2019a with TCSLD3.1 database[28] and, for an undercooling of 20 ± 2 K, all Ag_3Sn forms in eutectic regions between the β-Sn dendrites as shown in Fig. 2b. It can be clearly observed in Fig. 2c that the as-solidified eutectic Ag_3Sn particles are submicron and their shapes are elongated with an average aspect ratio of ~ 1.5, similar to the TEM study of Sn-3.5Ag BGA.[17] The size (equivalent circle diameter) of eutectic Ag_3Sn in the as-solidified joints was consistently ~ 120 nm, similar to the example in Fig. 2c.

One representative example of microstructural evolution during ageing at 125°C is shown in Fig. 3, using aligned BSE images. Six such fixed regions were investigated to obtain better statistics. Note that the few darker particles in the eutectic region are eutectic Cu_6Sn_5, which were not studied in this work. As the ageing time increases in Fig. 3b, c, d, e, f, g, h, and i, Ag_3Sn particles coarsened and coalesced simultaneously, and the growing particles remain confined within the original eutectic regions. Two boxes are marked in Fig. 3 to show particles that have coarsened (solid green box, where a single particle grows without touching its neighbours) or

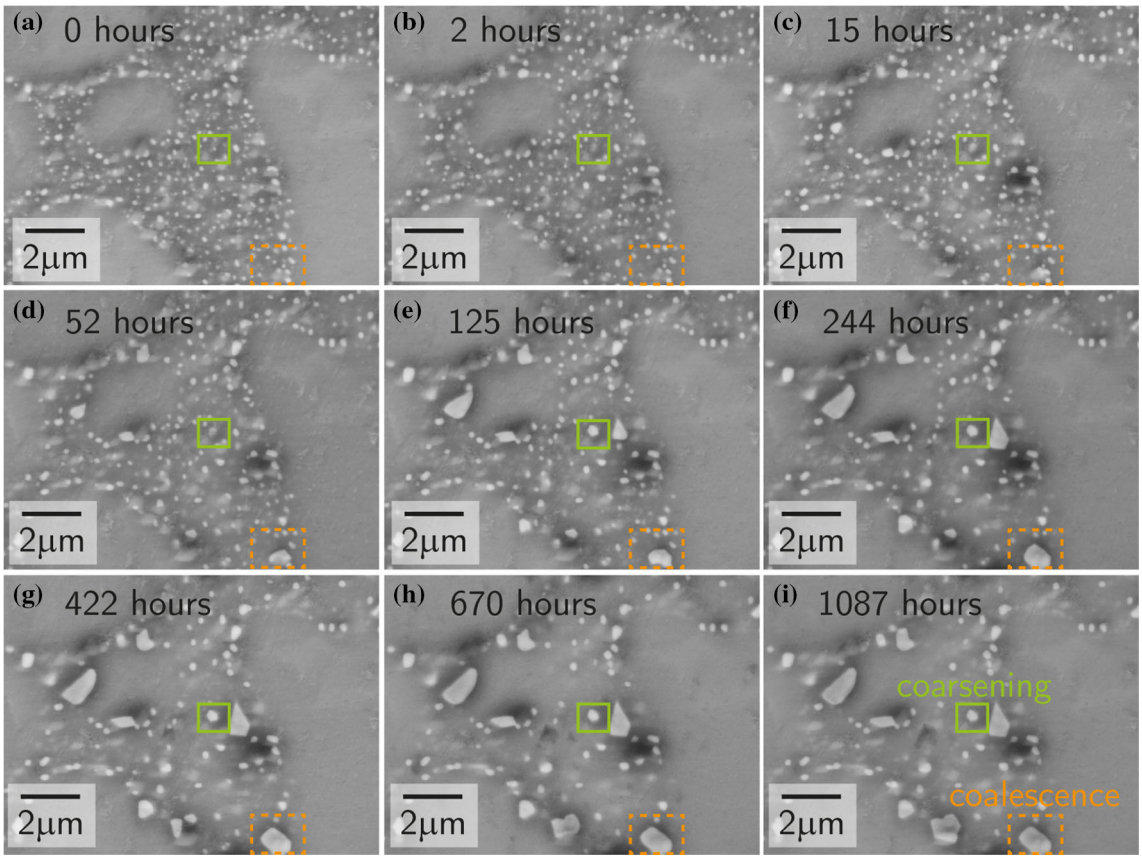

Fig. 3. Time-lapse BSE images of a SAC305/Cu joint during ageing at 125°C. (a) is the as-solidified microstructure. Ageing times are indicated in (b–i). Boxes show particles undergoing coarsening (green) and coalescence (orange) (Color figure online).

coalesced (dashed orange box, where multiple particles grow into each other and merge into a larger particle) during the 1087 h period. These two mechanisms are governed by different ripening processes, Ostwald ripening[29,30] and coalescence ripening.[31] A deeper quantification of these processes using numerous particles will be shown in "Quantification of Time-Lapse Images and Individual Particles" section using automated particle tracking.

Figure 4a compares the coarsening kinetics of the Ag_3Sn particles in the bulk and on the surface. Following the general kinetic relationship[21,32,33] in Eq 1, the phase size exponent n was measured to be very close to 3 and thus $t^{1/3}$ is plotted on the horizontal axis in Fig. 4a.

$$d^n - d_o^n = K_o \exp\left(-\frac{Q}{RT}\right)t \qquad (1)$$

where d is the particle size after ageing at temperature T for time t, d_o is the initial particle size. K_o is a constant and Q is the activation energy depending on the rate-controlling mechanism.[33] Note that the surface data come from re-measuring the same regions of a surface at different times, whereas the bulk data come from sectioning and measuring different samples at different times. The linear slopes of increasing d with $t^{1/3}$ are similar between the bulk and surfacing coarsening (Fig. 4a) implying that the free surface does not significantly change the coarsening kinetics of Ag_3Sn particles.

The histograms of scaled $r/\bar{r}^*$ ($\bar{r}^*$ being the mean Ag_3Sn particle size) and equivalent circle diameter (ECD) size distributions are shown in blue for the bulk location following 8-h ageing (Fig. 4b, d) and in red for the surface location after 15 h ageing (Fig. 4c, e). The shapes of the histograms are again very similar in both locations at the early stage of ageing (< 15 h in Fig. 4b–e) and maintained comparable throughout the ageing times investigated. For bulk coarsening, it is expected that the scaled histograms should be self-similar and time independent; the similarity between the histograms for surface and bulk coarsening further indicates that the free surface does not strongly affect coarsening.

Fitting the raw ECD particle size distributions using a lognormal function are included in Fig. 4d and e to further show the similarity between the histograms. There are in total > 8000 particles analyzed in the bulk and > 1400 particles on the surface in Fig. 4b, c, d, and e, although the number of particles decreases significantly due to the ripening processes. In Fig. 4b and c, two predicted

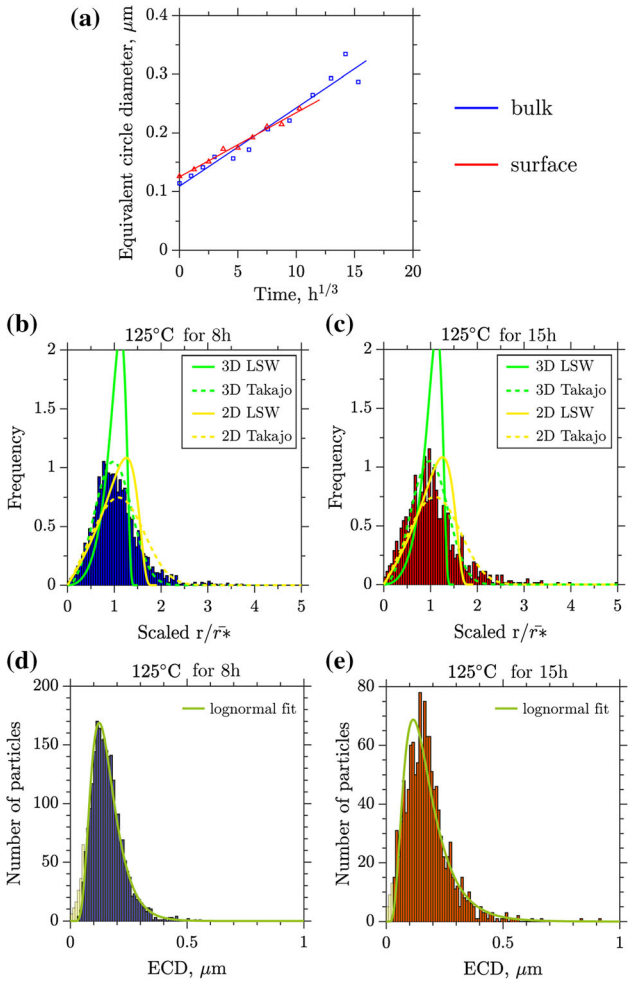

Fig. 4. (a) Coarsening kinetics of Ag_3Sn particles in the bulk solder (blue) and on the surface (red). The histogram of scaled particle size distribution and ECD distribution are shown for (b-c) bulk coarsening after 8 h and (d, e) surface coarsening after 15 h. The scaled distributions are overlaid with the LSW and Takajo (both in 3D and 2D) predictions, and the ECD distributions are fitted with lognormal functions (Color figure online).

distribution curves using the Lifshitz-Slyozov-Wagner (LSW)[29,30] model of pure Ostwald ripening and the Takajo model[31] incorporating coalescence, have been superimposed on the scaled histograms. The green distribution curves are the corresponding probability density functions for the LSW model[34] in Eq 2 and the Takajo model[31] in Eq 3:

$$F^{\mathrm{LSW}}(u) = \frac{1}{h_0}\frac{u^2}{(u+3)^{7/3}(3/2-u)^{11/3}}\exp\left(\frac{3}{2u-3}\right) \tag{2}$$

$$F^{\mathrm{Tkj}}(u) = 2.136u^2\exp\left(-0.7121u^3\right) \tag{3}$$

where u is the 3D scaled size $r/\bar{r}^*$. For the LSW function, the normalization constant h_o is determined numerically by the following condition[34]:

$$\int_0^{3/2} F^{\mathrm{LSW}}(u)\mathrm{d}u = 1 \rightarrow h_0 = 0.014419 \tag{4}$$

where 3/2 is the upper cut-off size (dimensionless) obtained from the LSW model.

For both models, the theoretical scaled 3D size distributions can be converted to scaled 2D size distributions that can be compared with the experimentally measured data from cross sections. The 3D to 2D conversion method is taken from Ref. 35, and the deduced scaled 2D particle distribution from the LSW and Takajo models are added as yellow curves in Fig. 4b and d. The 3D Takajo prediction curves seem a better fit to the experimental histogram peaks, while the 2D Takajo prediction curves provide better agreement with the right end of the spreading histograms, i.e. larger particles resulting from the coalescence of many particles. This is probably because, for the smaller particles near the peak location, the 2D and 3D difference in the cross section is negligible and could also be masked by the imaging segmentation uncertainties in smaller particles. Similarly, the 2D Takajo conversion is more appropriate and needed for larger particles in shapes of near spheres. On the other hand, the traditional 3D LSW prediction has a cut-off value of 1.5, which is invalid for all samples studied here. Hence, the overall matching using the LSW and Takajo (both 3D and 2D) models (Fig. 4b and d) confirms that particle coalescence is non-negligible for the growth of Ag_3Sn particles and the Takajo model offers a better description of the Ag_3Sn ripening process.

Quantification of Time-Lapse Images and Individual Particles

Figure 5 shows a post processed version of Fig. 3, which is a colourmap where each particle is coloured by its scaled size $r/\bar{r}^*$, where $\bar{r}^*$ is the mean particle size of all surface particles investigated from six different fixed regions. The background is coloured grey representing no particles being detected and is assumed to be β-Sn phase. One advantage of the colourmap is to visually demonstrate the particle spatial distribution in the 2D cross sections as well as the particle size distributions reflected by the colour key. It was repeatedly found that the larger particles are near-randomly distributed across the whole eutectic region and there is no strong evidence showing that Ag_3Sn particles tend to grow faster in the borders between eutectic regions and β-Sn dendrites. The colour key has an upper cut-off size of 2.5 and numerous yellowish particles are larger than the predicted upper cut-off size of 1.5 (LSW model) throughout the ageing times. This graphically shows that the tail of the particle size histograms for any ageing time do not follow the LSW theory, due to the coalescence of particles.

The coalescence or coarsening of all particles are not easily distinguishable in Figs. 3 and 5, and were only qualitatively reported in past time-lapse

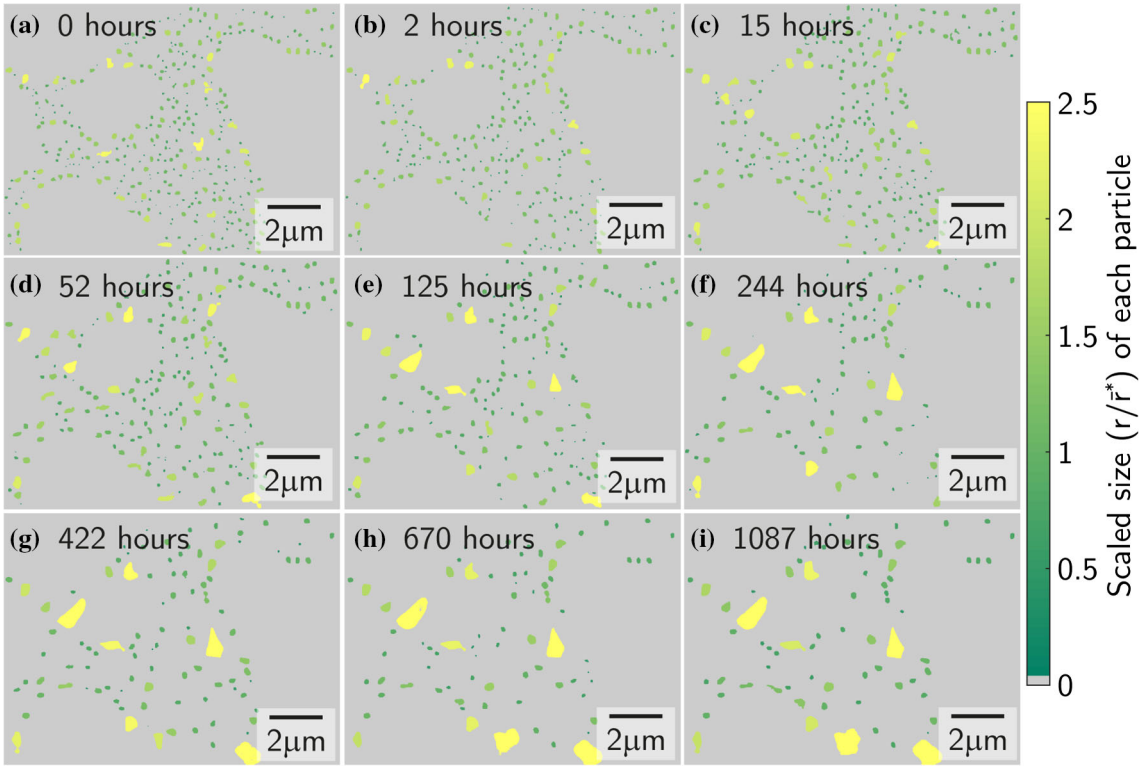

Fig. 5. For each ageing time at 125°C, individual Ag_3Sn particle is coloured by its scaled size $r/\bar{r}^*$, and $\bar{r}^*$ is the mean particle size from six different such regions. (a–i) Ageing time ranges from 0 to 1087 h (Color figure online).

studies.[11,25] In Ostwald ripening, normally bigger particles grow at the expense of smaller particles. However, some initially small particles may coalesce into a bigger particle during growth. The number of these coalesced initial particles were recorded for all evolving particles after various ageing times and are summarised as another colormap in Fig. 6. The colour key in Fig. 6 is defined by the number of initial eutectic particles that have coalesced into a large particle during ageing. The biggest red particle in the lower middle of Fig. 6i contains eight coalesced particles. Note that Fig. 6 is obtained from a different region to Fig. 3, containing more heavily coalesced particles than average. However, the coalescence is commonly seen in all time-lapse regions analysed. Figure 6 also shows that coalescence is observed as soon as 2 h after ageing started at 125°C and could have happened earlier (see the lighter blue particles in Fig. 6b). The coalescence also continues to occur until 1087 h ageing and may occur with Ostwald ripening for longer.

Based on colourmaps such as Figs. 5 and 6, the fraction of initial surface particles that became coalesced during ageing is quantified in Fig. 7. Figure 7a shows that initially there are more than 2000 Ag_3Sn surface particles being recorded in this time-lapse study, and the number of existing particles drops significantly to $\sim$ 500 particles (a $\sim$ 75% decrease) after 1087 h ageing at 125°C. The number of coalesced particles at each ageing time is plotted in Fig. 7b, which is different from the number of initial surface particles that coalesced as shown in Fig. 7d. Figure 7c is the ratio of coalesced particles over the number of existing particles at each time, effectively the ratio of datapoints in Fig. 7b over datapoints in Fig. 7a. This ratio follows a $t^{1/3}$ growth rate, and can be used to estimate the percentage of existing particles that have undergone coalescence at any given ageing time at 125°C, which is potentially also valid for bulk particles given the similarities discussed in Fig. 4. Figure 7e is the ratio of all datapoints in Fig. 7d over $\sim$ 2000, i.e. the number of total initial particles, representing the fraction of initial surface particles that became coalesced. The fraction in Fig. 7e would lead to a plateau value of $<$ 10%, indicating that the amount of initial Ag_3Sn particles that tend to be coalesced during ageing is about 10% of all Ag_3Sn particles present at the start of ageing.

To explore the behaviour of individual particles during time-lapse imaging, Fig. 8 tracks the evolution of selected individual surface particles in the form of contour lines created using a convex hull of the particle edges detected using the segmentation method in Fig. 1. The convex hull may slightly overestimate the actual measured particle size, but it helps to plot smoother contour lines for easier visual inspection of particle evolution in Fig. 8. Figure 8a overlays contour lines of all detected

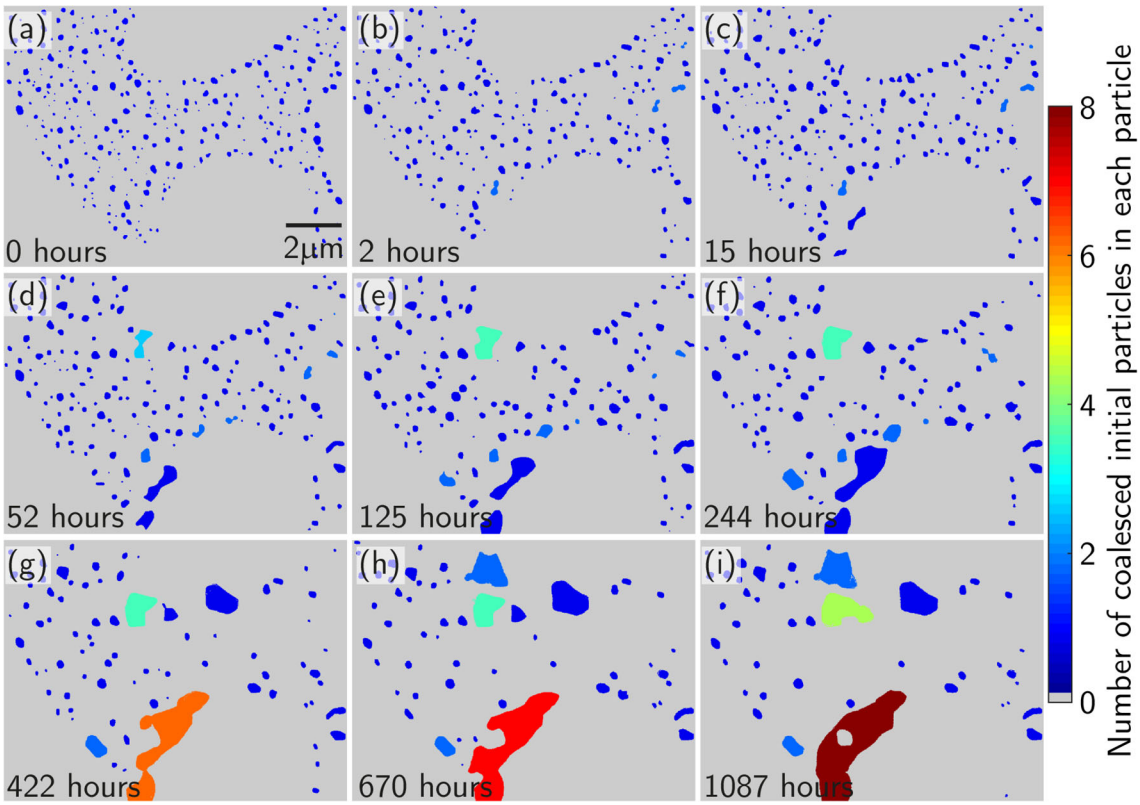

Fig. 6. For each ageing time at 125°C, individual Ag_3Sn particle is coloured by the number of initial eutectic particles in (a) it has coalesced during growth. (a–i) Ageing time ranges from 0 to 1087 h (Color figure online).

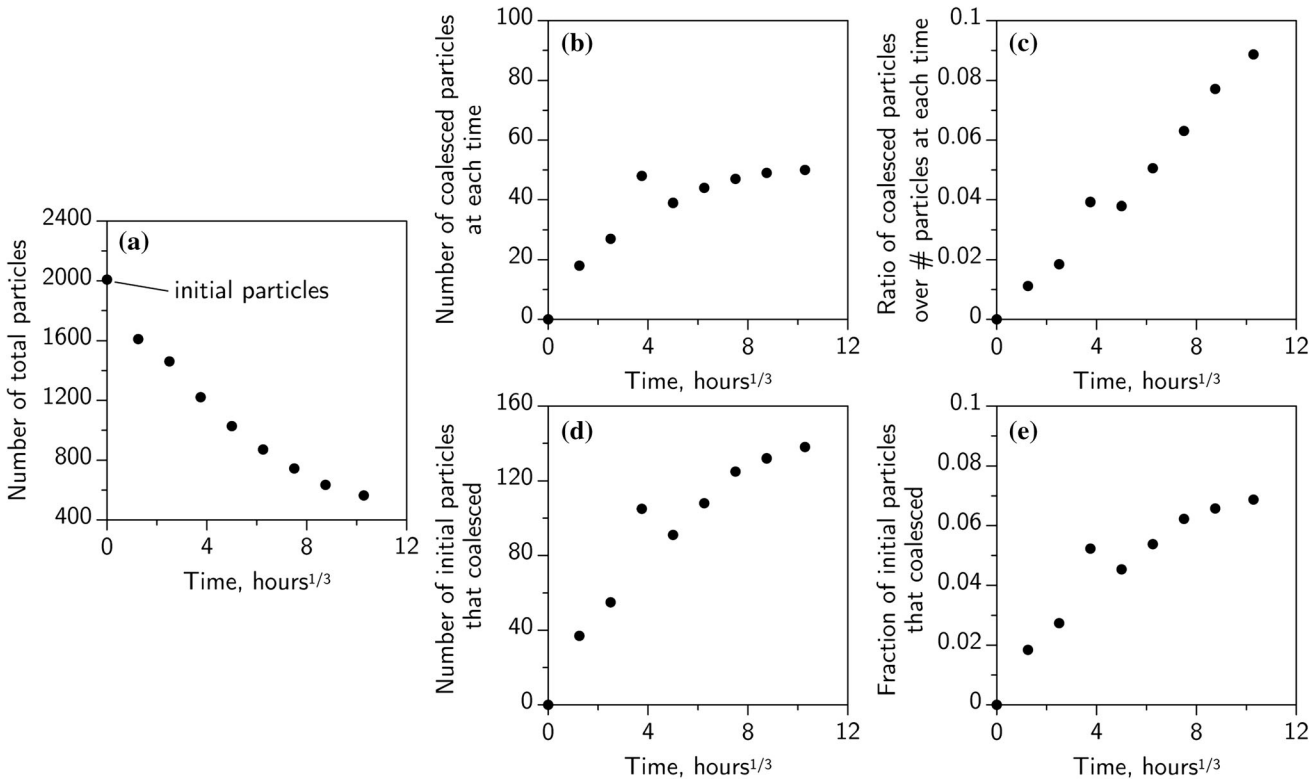

Fig. 7. (a) The number of total particles at each ageing time. (b) Number of coalesced particles at each ageing time. (c) The ratio of coalesced particles over total particles. (d) The number of initial particles that become coalesced. (e) Fraction of initial surface particles that become coalesced.

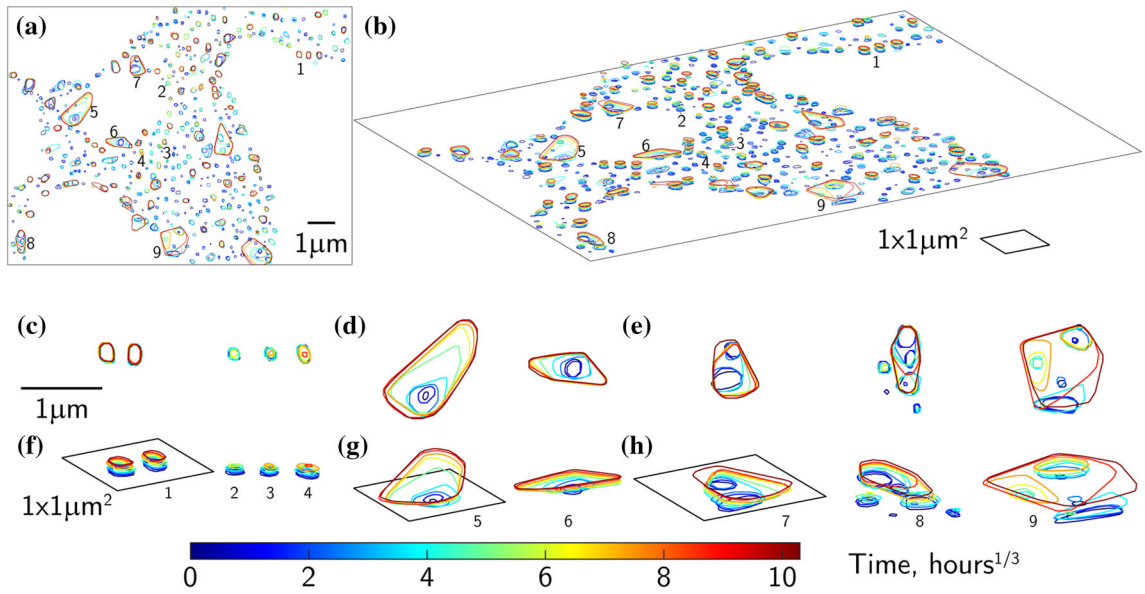

Fig. 8. Selected individual particles are tracked in contour lines. Contours lines are the convex hull of all particle edges detected from Fig. 3 and the contours from all nine frames in Fig. 3 have been overlaid together with different colours representing different ageing time. (a) and (c–e) are projected contour plots showing (c) unchanging and shrinking particles, (d) increasing particles and (e) coalescing particles. (b) and (f–h) are oriented at a random viewing angle for visual aid. Note that (c–e) share the same scale bar, as do (f–h).

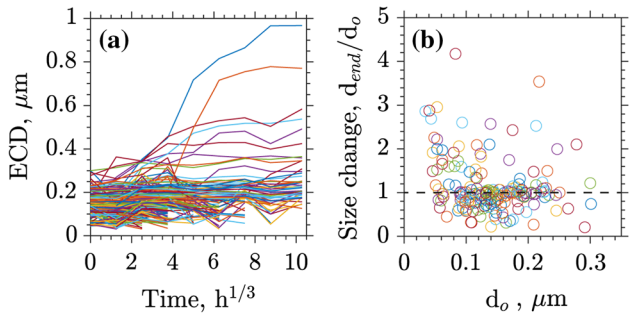

Fig. 9. (a) The size evolution of representative 184 particles in Fig. 3. ECD = equivalent circle diameter. (b) The ratio of final size and initial size of the same particles, > 1 means growing particles, < 1 means shrinking particles.

particle edges from the nine frames in Fig. 3, and the contour lines of each frame are assigned a colour representing the ageing time. Figure 8c, d, and e are selected particles from (a) and share the same scale bar. Figure 8b, f, g, and h are oriented at a random viewing angle for visual aid only. There are five particles, #1-4, in Fig. 8c with very similar initial sizes (see the blue contours in Fig. 8f). However, the left two particles (in Fig. 8a, #1) almost do not change size during ageing while the right three particles, #2-4, shrink. Moreover, the left particle in Fig. 8d, #5, is initially much smaller than the ones shown in Fig. 8c, but it grows much larger in the end.

As expected of Ostwald ripening, some of the Ag_3Sn particles in Fig. 8 grew and others shrank, but from these surface observations, there is no clear link between the initial size of a particle and whether it will grow or shrink. This is explored further in Fig. 9 which was plotted after tracking the size evolution of all 184 initial particles in Fig. 3. In Fig. 9a, the growth curves for all particles are shown. Some particles grow all the time, some remain nearly unchanged, while others shrink and then disappear.

The size change defined as the ratio of final size over initial size, d_{end}/d_o, is plotted against initial size in Fig. 9b. For a disappearing particle, the final size d_{end} is defined as its preceding size before it disappears, i.e. the end of shorter curves in Fig. 9a. Growing particles have a ratio larger than 1, and vice versa for the shrinking particles. As the initial size d_o increases, there is no trend for the initially larger particles to grow and no correlation can be found between the size change and the initial size d_o of the surface particles. Thus, it seems that, while the average coarsening kinetics presented in Fig. 4 are similar between the surface and bulk studies, the growth and shrinkage of individual particles requires information on the true 3D size of each particle in the subsurface which cannot be determined from the surface cross-section. It is also worth noting that the coarsening kinetics could also be affected by some preferential orientation relationship between Ag_3Sn and Sn, which will be explored in future work.

At the same time, analysis of individual particles in this surface study provides useful information on interplay between Ostwald ripening and the coalescence of particles. For example, in Fig. 8e, each of #7, #8 and #9 contain two or more particles of a range of initial sizes and some of these shrink in the early stages of coarsening. With increasing coarsening time, coalescence occurs among both growing

and shrinking particles, creating a larger particle with a jump in size. Such jumps can also be seen in Fig. 9a, which further highlights how calescence creates anomalously large Ag_3Sn particles compared with what would be expected of Ostwald ripening by an LSW mechanism.

CONCLUSIONS

The coarsening of Ag_3Sn particles in Sn-3Ag-0.5Cu/Cu joints at 125°C has been directly investigated using time-lapse imaging. A multi-step thresholding segmentation method and processed colourmaps have been developed to more efficiently and reproducibly evaluate microstructure evolution during isothermal ageing. The following conclusions can be drawn:

1. The initial size of Ag_3Sn particles was $\sim$ 120 nm in Sn-3Ag-0.5Cu/Cu joints with a β-Sn nucleation undercooling of 20 ± 2°C during continuous cooling at 0.33 K s^{-1}.
2. The coarsening kinetics and size distributions are found to be very similar for particles on the surface and in the bulk solders.
3. Coarsening occurred both by a classical Ostwald ripening (LSW-type) mechanism and by coalescence ripening.
4. Up to 10% of all initial particles coalesced during coarsening.
5. The Takajo model incorporating the coalescence process provides a better fit to the widening scaled particle size histograms measured during ageing than the LSW model.There are numerous Ag_3Sn particles with a scaled size larger than 1.5 (the upper cut-off value in the LSW model) throughout ageing, confirming that coalescence is non-negligible and can occur across the whole sample.
6. Coalescence produced large jumps in Ag_3Sn particle size and led to some anomalously large Ag_3Sn particles.

ACKNOWLEDGMENTS

We thank Martin Ng for valuable comments at the start of this project. The authors gratefully acknowledge the use of characterisation facilities within the Harvey Flower Electron Microscopy Suite, Department of Materials, Imperial College London. This work was funded by the UK EPSRC Grant EP/R018863/1.

CONFLICT OF INTEREST

The authors declare that they have no conflict of interest.

OPEN ACCESS

REFERENCES

1. S. Choi, J.G. Lee, F. Guo, T.R. Bieler, K.N. Subramanian, and J.P. Lucas, *JOM* 53, 22 (2001).
2. S. Terashima, Y. Kariya, T. Hosoi, and M. Tanaka, *J. Electron. Mater.* 32, 1527 (2003).
3. R.J. Coyle, K. Sweatman, and B. Arfaei, *JOM* 67, 2394 (2015).
4. A. Qasaimeh, Y. Jaradat, L. Wentlent, L. Yang, L. Yin, B. Arfaei, P. Borgesen, in *ECTC 2011* (2011), pp. 1775–1781.
5. T.R. Bieler, B. Zhou, L. Blair, A. Zamiri, P. Darbandi, F. Pourboghrat, T.K. Lee, and K.C. Liu, *J. Electron. Mater.* 41, 283 (2012).
6. L. Yin, L. Wentlent, L. Yang, B. Arfaei, A. Oasaimeh, and P. Borgesen, *J. Electron. Mater.* 41, 241 (2012).
7. J.K. Mattila, T.T. Kivilahti, in *TMS2013 Suppl. Proc.* (2013), pp. 401–411.
8. B. Arfaei, F. Mutuku, K. Sweatman, N. C. Lee, E. Cotts, R. Coyle, in *ECTC 2014* (2014), pp. 655–665.
9. J.B. Libot, J. Alexis, O. Dalverny, L. Arnaud, P. Milesi, and F. Dulondel, *Microelectron. Reliab.* 83, 64 (2018).
10. Y. Kariya, T. Hosoi, S. Terashima, M. Tanaka, and M. Otsuka, *J. Electron. Mater.* 33, 321 (2004).
11. N. Fu, S. Ahmed, J. C. Suhling, P. Lall, in *ECTC 2017* (2017), pp. 429–440.
12. F. Ochoa, J.J. Williams, and N. Chawla, *J. Electron. Mater.* 32, 1414 (2003).
13. J.M. Song, J.J. Lin, C.F. Huang, and H.Y. Chuang, *Mater. Sci. Eng. A* 466, 9 (2007).
14. S.K. Kang, W.K. Choi, D.-Y. Shih, D.W. Henderson, T. Gosselin, A. Sarkhel, C. Goldsmith, and K.J. Puttlitz, *J. Miner. Met. Mater. Soc.* 55, 61 (2003).
15. D.W. Henderson, T. Gosselin, A. Sarkhel, S.K. Kang, W.K. Choi, D.Y. Shih, C. Goldsmith, and K.J. Puttlitz, *J. Mater. Res.* 17, 2775 (2002).
16. I. Dutta, C. Park, and S. Choi, *Mater. Sci. Eng. A* 379, 401 (2004).
17. M. Kerr and N. Chawla, *Acta Mater.* 52, 4527 (2004).
18. I. Dutta, P. Kumar, and G. Subbarayan, *JOM* 61, 29 (2009).
19. C.M. Gourlay, S.A. Belyakov, Z.L. Ma, and J.W. Xian, *JOM* 67, 2383 (2015).
20. I. Dutta, *J. Electron. Mater.* 32, 201 (2003).
21. S.L. Allen, M.R. Notis, R.R. Chromik, and R.P. Vinci, *J. Mater. Res.* 19, 1417 (2004).
22. S. Choi, T.R. Bieler, J.P. Lucas, and K.N. Subramanian, *J. Electron. Mater.* 28, 1209 (1999).
23. W.K. Choi and H.M. Lee, *J. Electron. Mater.* 29, 1207 (2000).
24. L. Qi, J. Huang, H. Zhang, X. Zhao, H. Wang, and D. Cheng, *J. Mater. Eng. Perform.* 19, 129 (2010).
25. J. Wu, J. C. Suhling, P. Lall, in *ECTC 2019* (2019), pp. 1087–1098.
26. J.W. Xian, Z.L. Ma, S.A. Belyakov, M. Ollivier, and C.M. Gourlay, *Acta Mater.* 123, 404 (2017).
27. C.A. Schneider, W.S. Rasband, and K.W. Eliceiri, *Nat. Methods* 9, 671 (2012).

28. Thermo-Calc TCSLD Database version 3.1 (2019).
29. I.M. Lifshitz and V.V. Slyozov, *J. Phys. Chem. Solids* 19, 35 (1961).
30. C. Wagner, *Zeitschrift Für Elektrochemie Berichte Der Bunsengesellschaft Für Phys. Chemie* 65, 581 (1961).
31. S. Takajo, W.A. Kaysser, and G. Petzow, *Acta Metall.* 32, 107 (1984).
32. O.N. Senkov and M.M. Myshlyaev, *Acta Metall.* 34, 97 (1986).
33. K. Jung and H. Conrad, *J. Electron. Mater.* 30, 1303 (2001).
34. L. Ratke, P.W. Voorhees, *Growth and Coarsening* (2002).
35. L. Heinrich, *Image Anal. Stereol.* 26, 63 (2011).